analytical chemistry

pubs.acs.org/ac Article

Aggregation-Induced Electrochemiluminescence of Silica-Confined Tetraphenylethylene with Pd Nanocube-Loaded Co_3O_4 Nanosheets as a Coreaction Accelerator for Sensitive Bioanalysis

Yu Du, Rui Feng, Tingting Wu, Hongying Jia,* Bin Cai,* Huangxian Ju, and Qin Wei*

Cite This: *Anal. Chem.* 2024, 96, 20594−20601 Read Online

ACCESS | Metrics & More | Article Recommendations | Supporting Information

ABSTRACT: Aggregation-induced electrochemiluminescence (AIECL) provides a new approach for the development of novel electrochemiluminescence (ECL) strategies. Herein, a biosensor was constructed by incorporating 1,1,2,2-tetra(4-carboxylphenyl)ethylene (H_4TCPE) into a mesoporous silica nanosphere (MSN) to obtain a highly organized AIECL luminophore of (MSN-H_4TCPE) for signal antibody (Ab_2) labeling and using Pd nanocube (NC)-loaded Co_3O_4 nanosheets (NSs) (PdNCs/Co_3O_4NSs) as a novel coreaction accelerator. The confinement of H_4TCPE molecules in the MSN restricted the intramolecular rotation and thus enhanced the radiation transition of H_4TCPE. In addition, the PdNCs/Co_3O_4NSs exhibited efficient mutual conversion of the Co^{2+}/Co^{3+} redox couple with the perfect catalytic performance of PdNCs and facilitated the decomposition of the coreactant, leading to a substantial enhancement in ECL signal. Subsequently, the localization and fixation strategy with HWRGWVC (HWR) heptapeptides as a specific antibody immobilization agent was introduced, which further maintained the biological activity of the antibody on the PdNCs/Co_3O_4NSs and MSN-H_4TCPE surface and significantly improved the incubation performance. Benefiting from the perfect sensing strategy, the obtained ECL immunosensor revealed an admirable manifestation for the precise detection of neuron-specific enolase (NSE) with a broad concentration range of 1 fg/mL to 5 ng/mL and a detection limit of 0.33 fg/mL.

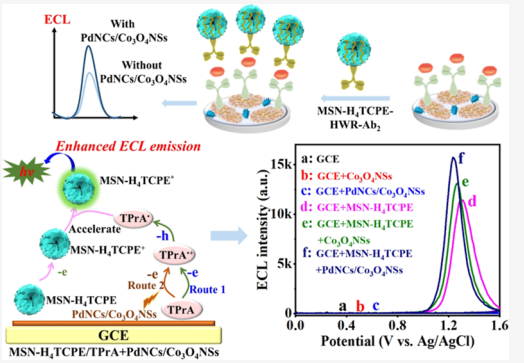

INTRODUCTION

Electrochemiluminescence (ECL), which refers to the light-emitting phenomenon triggered through the energetic electron-transfer reaction, has been considered as a promising technique according to the inherent superiorities of low background, admirable sensitivity, wide detection range, and admirable controllability.[1−3] The luminophores for ECL explorations include luminol,[4,5] ruthenium(II) complexes,[6,7] nanomaterials,[8,9] and metal clusters,[10,11] but most of them have limitations in modification due to their low stability, complicate procedures, and high cost. The effect of aggregation-induced ECL (AIECL) presents an intriguing mechanism as it broadens the application range of unfavorable ECL emitters and enhances the ECL emission through constraining intramolecular movements.[12−14] The emergence of AIE opens up a promising path for creating innovative biosensors. Recently, some researchers have explored the prevalent AIECL molecules, especially tetraphenylethylene (TPE) and its derivatives.[15,16] However, it is essential to encapsulate the AIECL molecules inside a cavity for the utilization of biosensors because it is challenging to decorate the small molecule onto the surface of the electrode. Inspired by this, our research group has previously attempted to encapsulate AIE molecules inside the protein nanocage of ferritin[13] and liposomes,[16] but their conductivities were inferior. Better than the protein nanocage and liposomes, mesoporous silica nanospheres (MSNs) display admirable potential to serve as effective carriers for encapsulating AIECL molecules owing to the characteristics of adjustable size for charge transfer, satisfying biocompatibility, and convenient modification. However, the limited contact between the intermediates of the coreactant and the AIECL molecule encapsulated inside the MSN restricts the performance, which becomes the main factor that influences the broad utilization and precise bioanalysis. Then, significant efforts should be implemented for boosting the efficiency of charge transfer along with promoting the performance of the AIECL molecule.

Fortunately, the excellent ECL performance by the acceleration of the coreactant has been realized through improving the electron transfer, which resulted in the formation of more electroactive radicals and promoted ECL

Received: September 26, 2024
Revised: November 9, 2024
Accepted: November 26, 2024
Published: December 17, 2024

https://doi.org/10.1021/acs.analchem.4c05219
Anal. Chem. 2024, 96, 20594−20601

Scheme 1. Construction of (A) PdNCs/Co_3O_4NSs-HWR; (B) MSN-H_4TCPE-HWR-Ab_2; (C) Fabricated Procedure of the Proposed ECL Immunosensor with MSN-H_4TCPE as the ECL Emitter and TPrA as the Coreactant

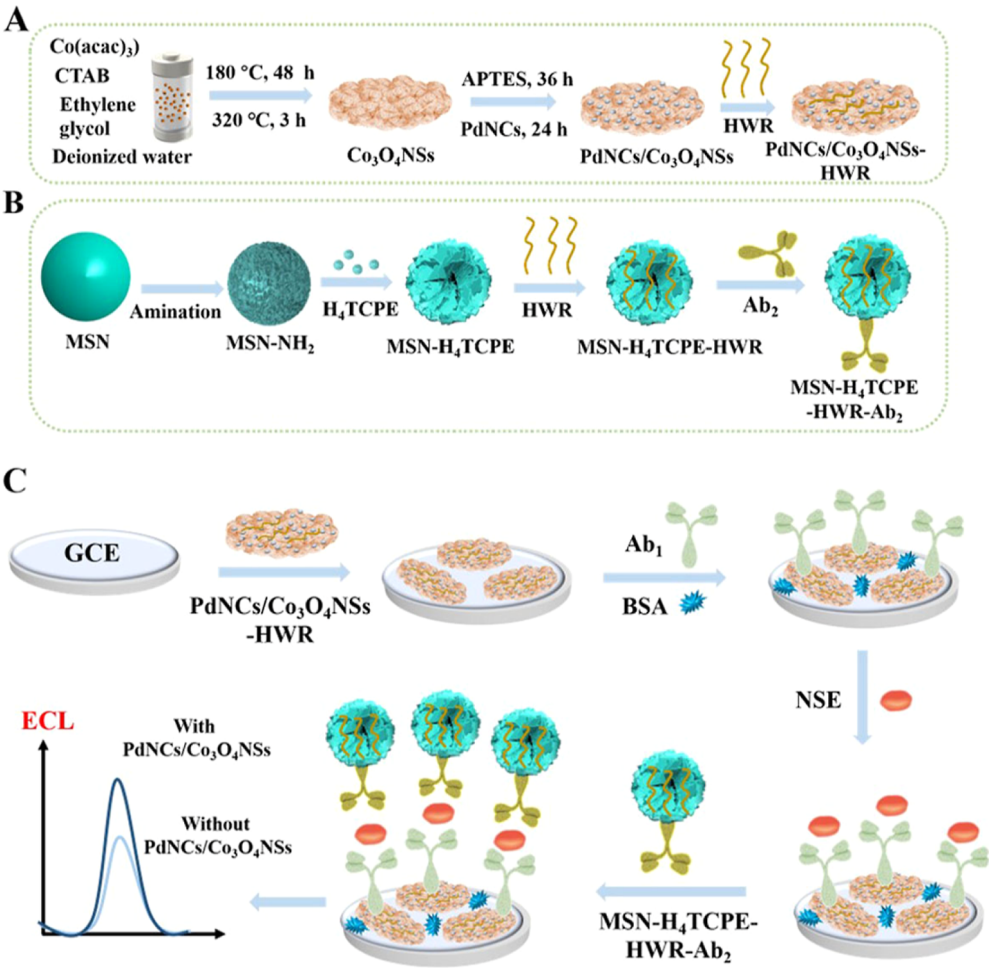

emission.[17] Interestingly, some nanomaterials, such as Co-2-MI-ZnTCPP,[18] CeO_2/Co_3O_4,[19] and $CuCo_2O_4$@Cu_2O,[20] were utilized as coreaction accelerators for promoting the ECL response, as their mutual conversion of Co^{2+}/Co^{3+}, Ce^{3+}/Ce^{4+}, and Cu^{2+}/Cu^{+} redox couples could efficiently enhance the generation of coreactant radicals.[19,21] However, the active sites of the aforementioned nanomaterials are not easily accessible because they are rare and concealed within the complex three-dimensional structure, thereby making the conversion of Co^{2+}/Co^{3+}, Ce^{3+}/Ce^{4+}, and Cu^{2+}/Cu^{+} challenging and greatly limiting improvements in ECL efficiency. Therefore, there is an urgent need for the development and utilization of innovative coreaction accelerators in the ECL system, in terms of both design and application. In this study, Co_3O_4 nanosheets (NSs) that possess numerous electroactive sites on their surface have been used as an innovative coreaction accelerator for the ECL system. By facilitating the efficient mutual transformation of the Co^{2+}/Co^{3+} redox couple, the nanosheets greatly enhanced the decomposition of coreactant tripropylamine (TPrA), leading to the generation of a substantial amount of $TPrA^{\bullet+}$, which significantly improved the ECL performance.

In view of the above discussion, we have first prepared an ECL strategy with PdNCs/Co_3O_4NSs as the coreaction accelerator to promote the AIECL signal of the MSN-H_4TCPE/TPrA system. First, PdNCs/Co_3O_4NSs were proposed as a basement for modifying the capture antibody (Ab_1) to assemble this detection platform. The efficient mutual transform of the Co^{2+}/Co^{3+} redox couple inside the composites of Co_3O_4NSs along with the Pd nanocubes (PdNCs) possessed high catalytic activity that could promote the electron transfer, leading to prominently enhanced ECL response. Considering the superiorities of biocompatibility, uniformity, and tunable pore size, MSNs were used as carriers for encapsulating H_4TCPE molecules, which could be covalently connected with the H_4TCPE for the AIECL of MSN-H_4TCPE. Meanwhile, to retain the bioactivity of the decorated antibody, the surface of PdNCs/Co_3O_4NSs and MSN-H_4TCPE was modified through HWRGWVC (HWR), a heptapeptide that selectively binds to the Fc segment of the antibody by a directed manner.[22,23] Our previous studies have shown that this targeted approach could enhance the efficiency of incubation while maintaining better bioactivity compared to conventional methods. Benefiting from the aforementioned discussion, the successful evolution of a sandwich-type ECL immunosensor was acquired by utilizing PdNCs/Co_3O_4NSs-HWR-Ab_1 as the platform of sensing and the AIECL molecule of MSN-H_4TCPE-HWR-Ab_2 as the ECL indicator. With the aim of supplying a practical target for early measurement of small cell lung carcinoma (SCLC), an ideal biomarker named neuron-specific enolase (NSE) was selected as an analyte.[24] The typical range of NSE in human serum is below 12 ng/mL;

https://doi.org/10.1021/acs.analchem.4c05219
Anal. Chem. 2024, 96, 20594−20601

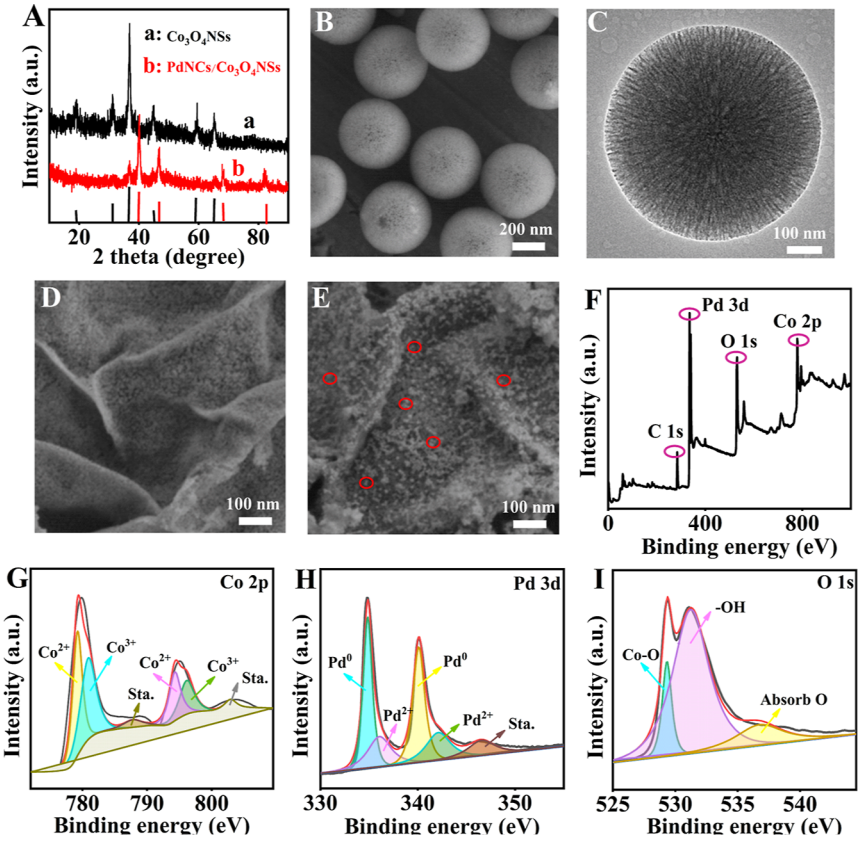

Figure 1. (A) XRD patterns of Co_3O_4NSs (a) and PdNCs/Co_3O_4NSs (b). (B) SEM image of MSN and (C) HRTEM image of MSN. (D, E) SEM images of Co_3O_4NSs (D) and PdNCs/Co_3O_4NSs (E). (F) XPS survey spectrum of PdNCs/Co_3O_4NSs. (G–I) High-resolution spectra of Co 2p (G) and Pd 3d (H) and O 1s (I) for PdNCs/Co_3O_4NSs.

however, the elevated levels are indicative of a higher likelihood of SCLC development. Consequently, assessing NSE levels is crucial for tracking the progression and evaluating the effectiveness of therapeutic interventions for SCLC in clinical settings.[25] This ECL immunosensor exhibited favorable linear signal within the content range of 1 fg/mL to 5 ng/mL and attained a low limit of detection (LOD) of 0.33 fg/mL.

EXPERIMENTAL SECTION

Fabrication Procedure of the ECL Immunosensor. The chemicals and materials, apparatus, and syntheses of PdNCs/Co_3O_4NSs-HWR and MSN-H_4TCPE-HWR-Ab_2 are presented in the Supporting Information (SI). Then, the synthesized process for the immunosensor is exhibited in Scheme 1. The glassy carbon electrode (GCE) was disposed cleanly for the next modification. First, PdNCs/Co_3O_4NSs-HWR (10 μL) was modified onto the surface of the GCE and cleaned by phosphate-buffered saline (PBS, 0.1 mol/L, pH 7.4). Next, 10 μL of Ab_1 solution (10 μg/mL) was decorated onto the PdNCs/Co_3O_4NSs-HWR surface and kept at 4 °C for 1 h. Afterward, the nonspecific active binding sites was sealed through bovine serum albumin (BSA) (3 μL, 0.1 wt %), and then 10 μL of diverse concentrations of NSE was modified onto the surface of the electrode with reacting for 1 h at 37 °C. Finally, the MSN-H_4TCPE-HWR-Ab_2 bioconjugate was used as the signal label to bond with NSE for completing the ECL immunosensor decoration.

Electrochemical and ECL Measurements. The cyclic voltammetry (CV) and ECL analyses were conducted for measurement. The corresponding ECL detection was obtained in PBS (0.1 mol/L, pH 7.4) including 0.01 mol/L TPrA used as the coreactant along with the following conditions: photomultiplier tube voltage (800 V), sweeping voltage (0–1.6 V), and sweeping rate (0.10 V/s).

RESULTS AND DISCUSSION

Characterizations of Co_3O_4NSs, PdNCs/Co_3O_4NSs, and MSNs. The detailed crystallographic structures of Co_3O_4NSs and PdNCs/Co_3O_4NSs were certified by X-ray diffraction (XRD) (Figure 1A). The diffraction peaks at 19.00°, 31.27°, 36.85°, 44.81°, 59.36°, and 65.24° were displayed, which could be attributed to the (111), (220), (311), (400), (511), and (440) planes of the Co_3O_4 phase (PDF#42-1467).[26] Meanwhile, the diffraction peaks at 40.12°, 46.66°, 68.12°, and 82.10° were assigned to the (111), (200), (220), and (311) planes of Pd (PDF#46-1043), which indicated that PdNCs were evenly dispersed on the surface of Co_3O_4NSs. The morphological characteristics of nanomaterials were observed by a field emission scanning electron microscope (FESEM). As displayed in Figure 1B, the MSN presented a uniform diameter of approximately 500 nm. It was an uncommon and well-organized nanoparticle that could serve as the sensing basement to enhance the consistency and durability for the immunosensor. Meanwhile, differentiable contrast under high voltages reveals the mesoporous structure located at the center of the nanosphere. To gain further insight into the internal channel, additional observations were made. The high-resolution transmission electron microscope (HRTEM) image of the MSN is displayed in Figure 1C. On

https://doi.org/10.1021/acs.analchem.4c05219
Anal. Chem. 2024, 96, 20594–20601

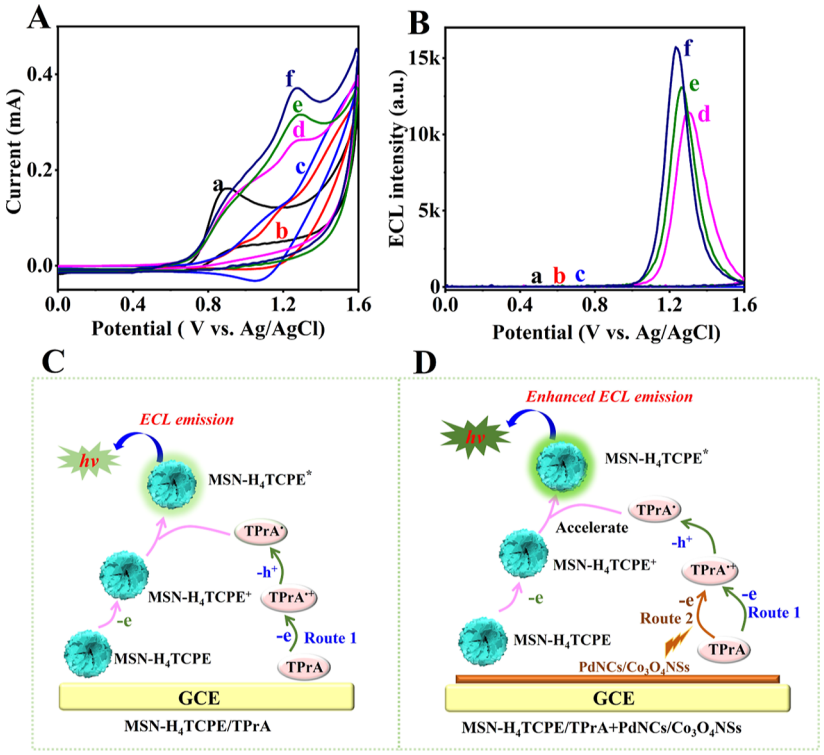

Figure 2. (A) CV curves and (B) ECL profiles for the MSN-H_4TCPE/TPrA system. (C, D) Mechanistic illustrations of the MSN-H_4TCPE/TPrA system (C) and MSN-H_4TCPE/TPrA system with PdNCs/Co_3O_4NSs as the coreaction accelerator (D).

account of its dense pores and ultrathin shell, the entire particle allowed effortless passage of an electron beam through it. The presence of this cavity supplies advantages in terms of confining and encapsulating AIECL luminophores. As displayed in Figure 1D, Co_3O_4NSs illustrated an outstanding and extensive nanosheet morphology. Meanwhile, as shown in the HRTEM image of Figure S1, the PdNCs displayed an average diameter of around 20 nm clearly. As displayed in the SEM images of Figure 1D,E, the PdNCs were proved to grow on the surface of Co_3O_4NSs uniformly with excellent dispersion. As shown in the energy-dispersive spectrometry (EDS) mapping and pattern of PdNCs/Co_3O_4NSs (Figures S2 and S3), it could be observed that the PdNCs/Co_3O_4NSs exhibited the desired surface morphology and structural composition.

The chemical components and elemental valence analysis of PdNCs/Co_3O_4NSs was evaluated by X-ray photoelectron spectroscopy (XPS) as exhibited in Figure 1F−I. As shown in Figure 1F, the full spectrum certified the presence of Co, O, and Pd. Furthermore, the high-resolution spectra of Co 2p, O 1s, and Pd 3d for PdNCs/Co_3O_4NSs are displayed in Figure 1G−I. Based on the spectrum of Co 2p (Figure 1G), it could be discovered that Co^{2+} and Co^{3+} coexisted inside the PdNCs/Co_3O_4NSs nanostructure.[27] Nevertheless, in the Pd 3d region (Figure 1H), the peaks were belonging to the Pd^{2+} and Pd^0 inside the PdNCs/Co_3O_4NSs.[28] Moreover, the corresponding spectrum of O 1s was broken up into three peaks (Figure 1I), which could be ascribed to Co with oxygen bonds, −OH structure, and the adsorbed O.

Enhancement of ECL Performance by PdNCs/Co_3O_4NSs. The important effect of PdNCs/Co_3O_4NSs in MSN-H_4TCPE/TPrA was explored. As displayed in Figure 2A,B, investigations with respect to isochronous CV and ECL measurements based on different situations were exhibited. The GCE did not generate an ECL value (Figure 2B, curve a). Next, after the decoration of Co_3O_4NSs (2 mg/mL) and PdNCs/Co_3O_4NSs (2 mg/mL) on the GCE, no ECL signals have been obtained inside PBS (pH 7.4) with 0.01 mol/L TPrA (Figure 2B, curves b and c). When MSN-H_4TCPE (2 mg/mL), MSN-H_4TCPE with Co_3O_4NSs, and PdNCs/Co_3O_4NSs with the uniform content modified onto the GCE, evident ECL responses along with the results of 11,425 au, 13,204 au, 15,913 au (Figure 2B curves d−f) could be acquired under the uniform conditions. The above consequences indicated that Co_3O_4NSs and PdNCs/Co_3O_4NSs could boost the ECL response of MSN-H_4TCPE, and the enhanced ECL response by PdNCs/Co_3O_4NSs was apparently higher than that by Co_3O_4NSs. Furthermore, the ECL emitting potentials were gradually decreasing (Figure 2B, curves d−f), and MSN-H_4TCPE with PdNCs/Co_3O_4NSs exhibited the downmost emission potential of 1.23 V. Moreover, the relevant CV consequences are displayed in Figure 2A. This GCE modified by MSN-H_4TCPE with PdNCs/Co_3O_4NSs displayed the strongest oxidic current, which indicated that PdNCs/Co_3O_4NSs played a significant character in improving the charge transfer.

Probable ECL Mechanism for Response Enhancement. According to the gained test consequences, the possible mechanism of the suggested ECL immunosensor has been exhibited in Figure 2C,D. When TPrA was used as the coreactant, the generation of $TPrA^{\bullet+}$ occurred near the electrode surface, leading to a favorable ECL performance (Figure 2C). Significantly, as PdNCs/Co_3O_4NSs took part in the ECL generation process (Figure 2D), the enhancement of $TPrA^{\bullet+}$ formation was clearly observed, leading to remarkable enlargement of the ECL response. Furthermore, the increased ECL response for MSN-H_4TCPE and PdNCs/Co_3O_4NSs was perhaps owing to the perfect catalytic performance of PdNCs/

https://doi.org/10.1021/acs.analchem.4c05219
Anal. Chem. 2024, 96, 20594−20601

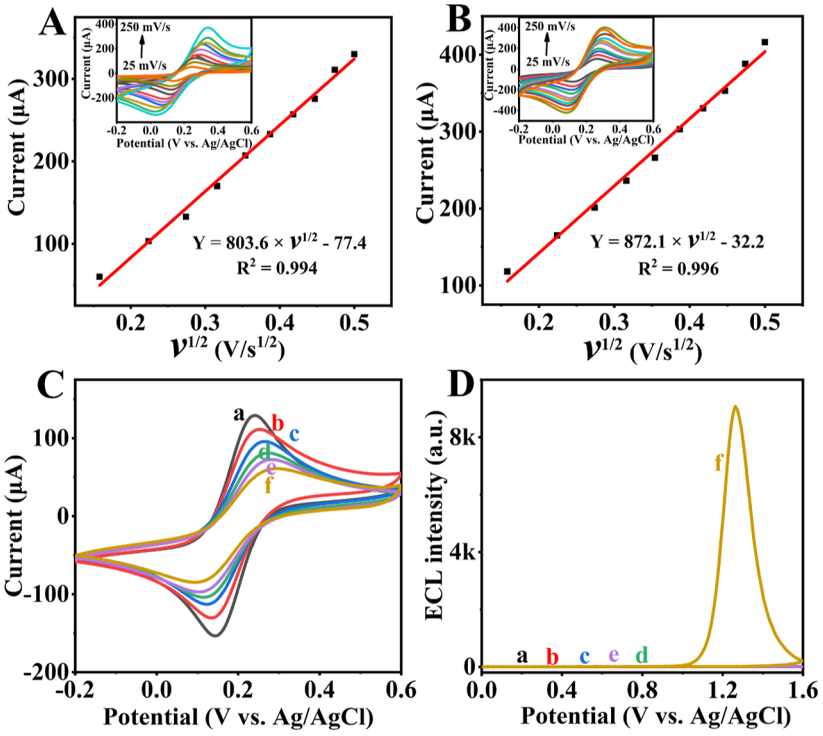

Figure 3. (A,B) CV curves and linear relations of the electrodes decorated with Co_3O_4NSs (A) and PdNCs/Co_3O_4NSs (B) in 5.0 mmol/L $Fe(CN)_6^{3-/4-}$ with the scan rate range of 25−250 mV/s. CV curves (C) and ECL profiles (D) of stepwise-modified electrodes by GCE (a), PdNCs/Co_3O_4NSs-HWR/GCE (b), Ab_1/PdNCs/Co_3O_4NSs-HWR/GCE (c), BSA/Ab_1/PdNCs/Co_3O_4NSs-HWR/GCE (d), NSE/BSA/Ab_1/PdNCs/Co_3O_4NSs-HWR/GCE (e), and MSN-H_4TCPE-HWR-Ab_2/NSE/BSA/Ab_1/PdNCs/Co_3O_4NSs-HWR/GCE (f).

Co_3O_4NSs as displayed in Figure S4. Electron paramagnetic resonance (EPR) based on the magnetic moment of unpaired electrons has been utilized for the qualitative detection of unpaired electrons. Typically, *N*-benzylidene-*tert*-butylamine *N*-oxide (PBN) serves as the spin trapping agent employed to verify the formation of $TPrA^{\bullet+}$ radicals.[29,30] As can be seen in Figure S4, a small signal was obtained in PBN, TPrA, and Co_3O_4NSs systems, which indicated the decomposition of TPrA by electrical excitation (curve a). In addition, the signal was further enhanced by the addition of PdNCs/Co_3O_4NSs (curve b), which indicated the perfect catalytic performance of the PdNCs. Resultantly, the ECL emission of the MSN-H_4TCPE/TPrA system was significantly enhanced by PdNCs/Co_3O_4NSs.

Therefore, considering the aforementioned analyses, the potential reaction mechanisms of the MSN-H_4TCPE/TPrA system could be summarized in the following manners (eqs 1−5). Initially, the electrochemical oxidation of MSN-H_4TCPE under an applied voltage led to the production of MSN-H_4TCPE$^+$. Simultaneously, the electrochemical oxidation of TPrA at the surface of the GCE resulted in the generation of $TPrA^{\bullet+}$ and $TPrA^{\bullet}$. Then, the MSN-H_4TCPE$^+$ species promptly reacted with the formed $TPrA^{\bullet}$ to generate highly active MSN-H_4TCPE*. Subsequently, the generated MSN-H_4TCPE* species underwent a transition to the ground condition, leading to the generation of ECL. However, for MSN-H_4TCPE/TPrA with the PdNCs/Co_3O_4NSs system, the PdNCs/Co_3O_4NSs triggered the generation of abundant $TPrA^{\bullet+}$ under the potential pulse, leading to a superb ECL response.

Enhanced ECL emission

$$\text{MSN-H}_4\text{TCPE-e}^- \rightarrow \text{MSN-H}_4\text{TCPE}^+ \quad (1)$$

$$\text{TPrA-e}^- \rightarrow (\text{PdNCs/Co}_3\text{O}_4\text{NSs})\text{TPrA}^{\bullet+}(\text{more}) \quad (2)$$

$$\text{TPrA}^{\bullet+} \rightarrow \text{TPrA}^{\bullet} + \text{H}^+ \quad (3)$$

$$\text{MSN-H}_4\text{TCPE}^+ + \text{TPrA}^{\bullet} \rightarrow \text{MSN-H}_4\text{TCPE}^* \quad (4)$$

$$\text{MSN-H}_4\text{TCPE}^* \rightarrow \text{MSN-H}_4\text{TCPE} + \text{hv} \quad (5)$$

Enhanced Electroactive Surface Area of PdNCs/Co_3O_4NSs. The electrochemical performance of Co_3O_4NSs would be evidently enhanced by the modification of PdNCs, which could be demonstrated by the improvement of the electroactive area. With the purpose of carrying out the exploration, GCEs were modified with Co_3O_4NSs and PdNCs/Co_3O_4NSs. All CV profiles were achieved through the prescriptive $Fe(CN)_6^{3-/4-}$ as a redox pair. Then, the acquired linear equations are $Y = 803.6 \times \nu^{1/2} - 77.4$ and $Y = 872.1 \times \nu^{1/2} - 32.2$, respectively. In view of the Randles−Sevcik equation[31,32]

$$I_p = (2.69 \times 10^5)AD^{1/2}n^{3/2}\nu^{1/2}c$$

It was known that I_p delegates the peak reductive value of $K_3Fe(CN)_6$, A indicates the area of the electrodes modified with different substrates, n is the amount of transferred charges during the redox procedure ($n = 1$), c is the content of applied $K_3Fe(CN)_6$ ($c = 5$ mmol/L), D represents the spread coefficient of $Fe(CN)_6^{3-/4-}$ ($D = 6.70 \times 10^{-6}$ cm^2/s at 25 °C), and ν indicates the CV scanning speed (V/s). Based on the Randles−Sevcik equation, the consequences of the Co_3O_4NS-modified GCE (Figure 3A) and PdNCs/Co_3O_4NS-(Figure 3B)-modified GCE were 16.0 and 22.1 mm^2, respectively, which certified that PdNCs/Co_3O_4NSs possessed

https://doi.org/10.1021/acs.analchem.4c05219
Anal. Chem. 2024, 96, 20594−20601

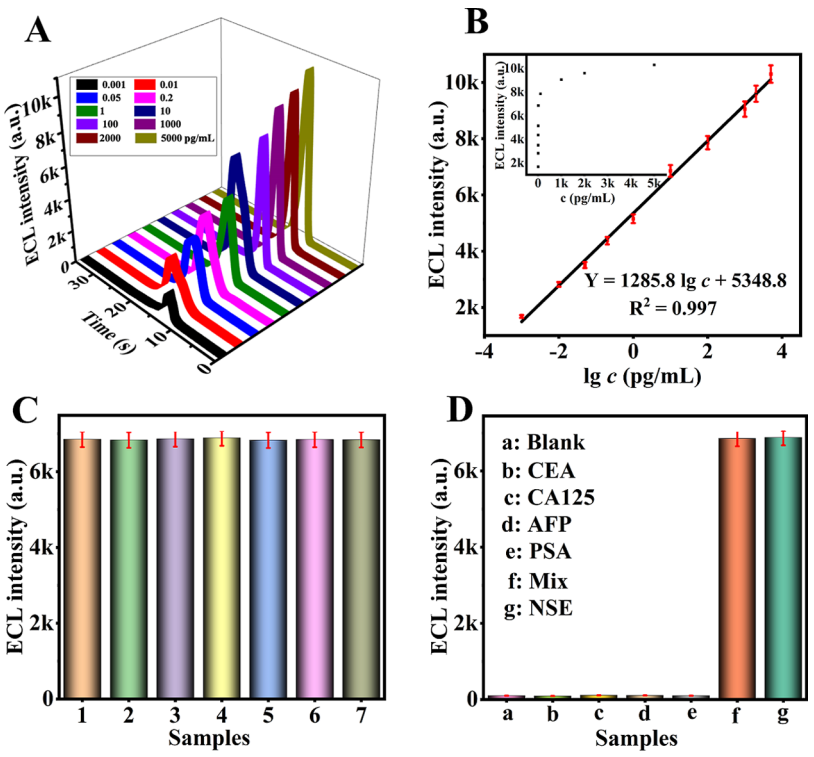

Figure 4. (A) ECL intensity−time curves and (B) relevant calibration profile of the prepared immunosensor at different concentrations of NSE (1 fg/mL to 5 ng/mL) in the 0.1 mol/L PBS (pH 7.4) including 0.01 mol/L TPrA. (C) Reproducibility of the ECL immunosensor to the analysis of seven electrodes and (D) selectivity of the ECL immunosensor to the disparate targets, inset of 4B: the relation between the ECL response and content of NSE.

the electroactive area and charge transfer speed was better for catalytic reaction.

Feasibility of ECL Immunosensor. CV is a significant technique for carrying out the construction process of the immunosensor. As revealed in Figure 3C, the depressed peak current and increased peak potential separation were exhibited after the continuous modification of the electrode, certifying the obstruction of electron transfer and perfect construction of the fabricated immunosensor. Moreover, the ECL profiles have been certified as a perfect electrochemical manner for observing the preparation procedure of the immunosensor. As displayed in Figure 3D, no ECL signals were obtained from GCE (curve a), PdNCs/Co_3O_4NSs-HWR/GCE (curve b), Ab_1/PdNCs/Co_3O_4NSs-HWR/GCE (curve c), BSA/Ab_1/PdNCs/Co_3O_4NSs-HWR/GCE (curve d), and NSE/BSA/Ab_1/PdNCs/Co_3O_4NSs-HWR/GCE (curve e) with the existence of TPrA. However, MSN-H_4TCPE-HWR-Ab_2/NSE/BSA/Ab_1/PdNCs/Co_3O_4NSs-HWR/GCE (curve f) displayed the obvious ECL signal under the same condition, which demonstrated the successful construction of the immunosensor.

Optimization of the Detection Conditions. The fitted pH was very important to construct the ECL immunosensor. Then, after researching the property of the ECL immunosensor toward diverse pH from 5.5 to 8.5, pH 7.4 was used in the experiment as displayed in Figure S5A. TPrA was applied as the coreactant, and the ECL response obtained excellent consequence while the concentration of TPrA was 0.01 mol/L (Figure S5B). As observed in Figure S5C, the ECL response was promoted along with enhanced content of PdNCs/Co_3O_4NSs below 2.5 mg/mL and decreased after the concentration surpassed 2.5 mg/mL. Then, 2.5 mg/mL PdNCs/Co_3O_4NSs was utilized in this ECL experiment. Eventually, the incubation time of Ab_2 bioconjugates is exhibited in Figure S5D, and the consequences indicated a best reaction time of 60 min. Besides, the incubation time of the Ab_2 bioconjugates was less than in other methods because of the site-oriented decoration for antibodies by HWR, thus enhancing their incubating response.

Performance of the ECL Immunosensing on NSE. Under the optimizations of related detected situations (Figure S5), the ECL immunosensor was studied through modifying various concentrations of NSE. As viewed in Figure 4A, the achieved ECL signals enhanced sequentially while the concentrations of NSE promoted from 1 fg/mL to 5 ng/mL. Furthermore, as observed from Figure 4B, the acquired ECL responses displayed a wonderful linear relation with the logarithm of NSE, and the achieved linear regression equation was $Y = 1285.8 \lg c + 5348.8$ ($R^2 = 0.997$). Meanwhile, the obtained LOD for this prepared immunosensor was 0.33 fg/mL (S/N = 3), exhibiting better sensitivity than the prior research (Table S1).

Furthermore, reproducibility, selectivity, and stability were also crucial factors for evaluating the analytical property of this immunosensor. As observed in Figure 4C, the performance for seven prepared ECL immunosensors was detected at 10 pg/mL of NSE to verify wonderful reproducibility with a relative standard deviation (RSD) of 1.1%. Then, the selectivity was investigated, and carcinoembryonic antigen (CEA), carcinoma antigen 125 (CA125), alpha-fetoprotein (AFP), and prostate specific antigen (PSA) were used as the interferences. The responses of the above interferences at the content 100 times that of NES were about near that of the blank. The mixture (10 pg/mL NSE and 1 ng/mL interferences) displayed almost the

https://doi.org/10.1021/acs.analchem.4c05219
Anal. Chem. 2024, 96, 20594−20601

same ECL signal as the NSE, which showed superb selectivity (Figure 4D). In addition, the stability was obtained by storing the prepared immunosensor for 3 weeks, displaying an ECL signal that was 87% the original signal, indicating the perfect stability.

Serum Sample Analysis. With the purpose of demonstrating the clinical performance of the constructed immunosensor, it has been utilized to detect the content of NSE and confirm exactitude by the standard addition approach. As shown in Table 1, the obtained RSD was less than 5%, and then the recovery was within 98−102%, which verified the potential utilization of this prepared strategy in clinical determination.

Table 1. Recovery Results Achieved from the ECL Immunosensor

initial content (pg/mL)	added content (pg/mL)	obtained content (pg/mL)	RSD (n = 5, %)	recovery (%)
0.50	0.50	0.98, 1.04, 1.03, 1.02, 0.99	2.56	102.4
	1.00	1.48, 1.45, 1.52, 1.47, 1.49	1.75	98.2
	1.50	2.07, 2.05, 1.97, 1.98, 2.06	2.33	101.7

CONCLUSIONS

In this study, PdNCs/Co_3O_4NSs, a perfect coreactant accelerator prepared for boosting the AIECL performance of the MSN-H_4TCPE/TPrA system, were constructed and applied in the immunosensor for NSE analysis. The research findings have verified the capacity of MSNs to effectively confine AIECL molecules and established the groundwork for the synthesis of functional nanomaterials. Notably, the PdNCs/Co_3O_4NSs were synthesized as a coreaction accelerator and exhibited remarkable capabilities in generating a larger number of $TPrA^{\bullet+}$ radicals. This was facilitated by their efficient mutual conversion of the Co^{2+}/Co^{3+} redox couple and the excellent catalytic performance with the abundant active sites. Meanwhile, the polypeptide HWR effectively enhanced the incubation characteristics, greatly promoting the performance of the immunosensor. Moreover, the developed immunosensor was successfully achieved by ultrasensitive analysis of NSE within a wide concentration range of 1 fg/mL to 5 ng/mL, realizing a remarkable LOD of 0.33 fg/mL. This approach not only offers novel perspectives on the construction of nanosheets for enhancing the ECL response of the MSN-H_4TCPE/TPrA system but also supplies precious acquaintances into the use of AIECL functional materials as the ECL emitter for enhancing the sensitivity.

ASSOCIATED CONTENT

Supporting Information

The Supporting Information is available free of charge at https://pubs.acs.org/doi/10.1021/acs.analchem.4c05219.

Chemicals and materials; apparatus; preparation of MSN, MSN-H_4TCPE, MSN-H_4TCPE-HWR-Ab_2 bioconjugates, PdNCs, Co_3O_4NSs, PdNCs/Co_3O_4NSs, and PdNCs/Co_3O_4NSs-HWR; HRTEM of PdNCs; EDS mapping and pattern of PdNCs/Co_3O_4NSs; EPR spectra; optimization of the detection conditions; comparison of analytical performances for NSE detection; and references (PDF)

AUTHOR INFORMATION

Corresponding Authors

Hongying Jia − *Collaborative Innovation Center for Green Chemical Manufacturing and Accurate Detection, School of Chemistry and Chemical Engineering, University of Jinan, Jinan 250022, PR China*; Email: Hongying187@163.com

Bin Cai − *School of Chemistry and Chemical Engineering, Shandong University, Jinan 250100, China*; orcid.org/0000-0002-3263-0395; Email: bin.cai@sdu.edu.cn

Qin Wei − *Collaborative Innovation Center for Green Chemical Manufacturing and Accurate Detection, School of Chemistry and Chemical Engineering, University of Jinan, Jinan 250022, PR China; Department of Chemistry, Sungkyunkwan University, Suwon 16419, Republic of Korea*; orcid.org/0000-0002-3034-8046; Email: sdjndxwq@163.com

Authors

Yu Du − *School of Water Conservancy and Environment, University of Jinan, Jinan 250022 Shandong, China*; orcid.org/0000-0002-9002-8845

Rui Feng − *School of Water Conservancy and Environment, University of Jinan, Jinan 250022 Shandong, China*; orcid.org/0000-0001-5918-8712

Tingting Wu − *Collaborative Innovation Center for Green Chemical Manufacturing and Accurate Detection, School of Chemistry and Chemical Engineering, University of Jinan, Jinan 250022, PR China*

Huangxian Ju − *Collaborative Innovation Center for Green Chemical Manufacturing and Accurate Detection, School of Chemistry and Chemical Engineering, University of Jinan, Jinan 250022, PR China*; orcid.org/0000-0002-6741-5302

Complete contact information is available at: https://pubs.acs.org/10.1021/acs.analchem.4c05219

Notes

The authors declare no competing financial interest.

ACKNOWLEDGMENTS

This project was supported by the National Natural Science Foundation of China (22304060, 22274062, and 22206056), the Natural Science Foundation of Shandong Province (ZR2023QB019 and ZR2022QB117), and the China Postdoctoral Science Foundation (2023M741359).

REFERENCES

(1) Wang, Y. G.; Zhao, G. H.; Chi, H.; Yang, S. H.; Niu, Q. F.; Wu, D.; Cao, W.; Li, T. D.; Ma, H. M.; Wei, Q. *J. Am. Chem. Soc.* **2021**, *143* (1), 504−512.

(2) Wang, N. N.; Gao, H.; Li, Y. Z.; Li, G. M.; Chen, W. W.; Jin, Z. C.; Lei, J. P.; Wei, Q.; Ju, H. X. *Angew. Chem., Int. Ed.* **2021**, *60* (1), 197−201.

(3) Jia, H. Y.; Yang, L.; Dong, X.; Zhou, L. M.; Wei, Q.; Ju, H. X. *Anal. Chem.* **2022**, *94* (4), 2313−2320.

(4) Lai, W. J.; Li, J. J.; Jiang, M. Z.; Li, P. L.; Wang, M.; Ma, C. Y.; Zhao, C. L.; Qi, Y.; Hong, C. L. *Anal. Chem.* **2023**, *95* (18), 7109−7117.

(5) Guo, J. N.; Xie, M. S.; Du, P. Y.; Liu, Y.; Lu, X. Q. *Anal. Chem.* **2021**, *93* (30), 10619−10626.

(6) Xia, M.; Zhou, F.; Feng, X.; Sun, J.; Wang, L.; Li, N.; Wang, X.; Wang, G. *Anal. Chem.* **2021**, *93* (32), 11284−11290.

(7) Bai, W. Q.; Cui, A. P.; Liu, M. Z.; Qiao, X.; Li, Y.; Wang, T. *Anal. Chem.* **2019**, *91* (18), 11840−11847.

(8) Zhu, D.; Zhang, Y.; Bao, S. S.; Wang, N. N.; Yu, S. Q.; Luo, R. G.; Ma, J.; Ju, H. X.; Lei, J. P. *J. Am. Chem. Soc.* **2021**, *143* (8), 3049−3053.
(9) Jin, Z. C.; Zhu, X. R.; Wang, N. N.; Li, Y. F.; Ju, H. X.; Lei, J. P. *Angew. Chem., Int. Ed.* **2020**, *59* (26), 10446−10450.
(10) Jia, H. Y.; Yu, S. Q.; Yang, L.; Wei, Q.; Ju, H. X. *ACS Appl. Nano Mater.* **2021**, *4* (3), 2657−2663.
(11) Weng, Z.; Li, Z.; Zhang, Y.; Zhang, M.; Huang, Z.; Chen, W.; Peng, H. *Anal. Chem.* **2022**, *94* (45), 15896−15901.
(12) Liu, J. L.; Zhang, J. Q.; Tang, Z. L.; Zhuo, Y.; Chai, Y. Q.; Yuan, R. *Chem. Sci.* **2019**, *10* (16), 4497−4501.
(13) Yang, L.; Sun, X.; Wei, D.; Ju, H. X.; Du, Y.; Ma, H. M.; Wei, Q. *Anal. Chem.* **2021**, *93* (3), 1553−1560.
(14) Cui, L.; Zhao, M. H.; Li, C. C.; Wang, Q. B.; Luo, X. L.; Zhang, C. Y. *Anal. Chem.* **2021**, *93* (5), 2974−2981.
(15) Jia, Y.; Du, Y.; Ru, Z. Z.; Fan, D. W.; Yang, L.; Ren, X.; Wei, Q. *Anal. Chem.* **2023**, *95* (16), 6725−6731.
(16) Jia, Y.; Ren, X.; Zhang, X. Y.; Wu, D.; Ma, H. M.; Li, Y. Y.; Wei, Q. *Anal. Chem.* **2023**, *95* (24), 9139−9144.
(17) Zhou, Y.; Chai, Y. Q.; Yuan, R. *Anal. Chem.* **2019**, *91* (22), 14618−14623.
(18) Liang, J.; Xu, Q.; Teng, X.; Guan, W.; Lu, C. *Anal. Chem.* **2020**, *92* (1), 1628−1634.
(19) Zhao, L.; Song, X. Z.; Ren, X.; Fan, D. W.; Wei, Q.; Wu, D. *Anal. Chem.* **2021**, *93* (24), 8613−8621.
(20) Jia, H. Y.; Li, J. S.; Yang, L.; Fan, D. W.; Kuang, X.; Sun, X.; Wei, Q.; Ju, H. X. *Anal. Chem.* **2022**, *94* (19), 7132−7139.
(21) Jia, Y.; Yang, L.; Xue, J. W.; Ren, X.; Zhang, N.; Fan, D. W.; Wei, Q.; Ma, H. M. *Biosens. Bioelectron.* **2019**, *144*, 111676.
(22) Song, X. Z.; Shao, X. R.; Dai, L.; Fan, D. W.; Ren, X.; Sun, X. J.; Luo, C. N.; Wei, Q. *ACS Appl. Mater. Interfaces* **2020**, *12* (8), 9098−9106.
(23) Yang, L.; Jia, Y.; Wu, D.; Zhang, Y.; Ju, H. X.; Du, Y.; Ma, H. M.; Wei, Q. *Anal. Chem.* **2019**, *91* (21), 14066−14073.
(24) Chen, Y.; Ge, X. Y.; Cen, S. Y.; Wang, A. J.; Luo, X. l.; Feng, J. J. *Sens. Actuators, B* **2020**, *311*, 127931.
(25) Huang, X. Y.; Miao, J. C.; Fang, J. L.; Xu, X. T.; Wei, Q.; Cao, W. *Talanta* **2022**, *239*, 123075.
(26) Poonguzhali, R. V.; Kumar, E. R.; Srinivas, C.; Alshareef, M.; Aljohani, M. M.; Keshk, A. A.; El-Metwaly, N. M.; Arunadevi, N. *Sens. Actuators, B* **2023**, *377*, 133036.
(27) Zheng, J. H.; Liu, X. Y.; Zhang, L. *Chem. Eng. J.* **2020**, *389*, 124339.
(28) Lüsi, M.; Erikson, H.; Tammeveski, K.; Treshchalov, A.; Kikas, A.; Piirsoo, H.-M.; Kisand, V.; Tamm, A.; Aruväli, J.; Solla-Gullón, J.; Feliu, J. M. *Electrochim. Acta* **2021**, *394*, 139132.
(29) Li, J. H.; Liu, J. L.; Zhang, X. L.; Zhu, X. C.; Yuan, R.; Chai, Y. Q. *Anal. Chem.* **2023**, *95* (8), 4131−4137.
(30) Li, J. S.; Wang, X. Q.; Liu, W.; Li, X. J.; Yang, L.; Ma, H. M.; Wu, R. D.; Wei, Q. *Sens. Actuators, B* **2021**, *346*, 130581.
(31) Li, L. L.; Liu, K. P.; Yang, G. H.; Wang, C. M.; Zhang, J. R.; Zhu, J. J. *Adv. Funct. Mater.* **2011**, *21* (5), 869−878.
(32) Wang, H. J.; Yuan, Y. L.; Zhuo, Y.; Chai, Y. Q.; Yuan, R. *Anal. Chem.* **2016**, *88* (4), 2258−2265.

https://doi.org/10.1021/acs.analchem.4c05219
Anal. Chem. 2024, 96, 20594−20601